JCB: **Article**

Epiblast integrity requires CLASP and Dystroglycan-mediated microtubule anchoring to the basal cortex

Yukiko Nakaya, Erike W. Sukowati, and Guojun Sheng

Laboratory for Early Embryogenesis, Institute of Physical and Chemical Research (RIKEN) Center for Developmental Biology, Chuo-Ku Kobe, Hyogo 650-0047, Japan

Amniote epiblast cells differentiate into mesoderm and endoderm lineages during gastrulation through a process called epithelial-to-mesenchymal transition (EMT). Molecular regulation of gastrulation EMT is poorly understood. Here we show that epiblast epithelial status was maintained by anchoring microtubules to the basal cortex via CLIP-associated protein (CLASP), a microtubule plus-end tracking protein, and Dystroglycan, a transmembrane protein that bridges the cytoskeleton and basement membrane (BM). Mesoderm formation required down-regulation of CLASP and Dystroglycan, and reducing CLASP activity in pregastrulation epiblast cells caused ectopic BM breakdown and disrupted epiblast integrity. These effects were mediated through the CLASP-binding partner LL5. Live-imaging using EB1–enhanced GFP (eGFP) revealed that reducing CLASP and LL5 levels in the epiblast destabilized basal microtubules. We further show that Dystroglycan is localized to basolateral membrane in epiblast cells. Basal but not lateral localization of Dystroglycan was regulated by CLASP. We propose that epiblast–BM interaction requires CLASP- and Dystroglycan-mediated cortical microtubule anchoring, the disruption of which initiates gastrulation EMT.

Introduction

Epithelial-to-mesenchymal transition (EMT) is a phenomenon in which cells change their shape and intercellular organization from an epithelial type to a mesenchymal one. Correct execution of EMT and its reverse process MET is vital for tissue morphogenesis during animal development, and their abnormal reinitiation leads to organ fibrosis and tumor metastasis (Moreno-Bueno et al., 2008; Kalluri and Weinberg, 2009; Thiery et al., 2009; Kerosuo and Bronner-Fraser, 2012; Lim and Thiery, 2012). Cell-biologically, EMT has been well characterized as a multistep process that includes dissolution of local basement membrane (BM), loss of the epithelial polarity and tight junctions (TJs), switch of the adherens junction (AJ) subtypes, and mesenchymal cell migration. Molecularly, transcription factors such as Snail, Twist, Zeb1, and Zeb2 are viewed as key mediators between signaling input (e.g., TGFβ, FGF, EGF, and HGF) on one hand and cell biological output on the other, measured mainly by E-cadherin down-regulation and loss of epithelial polarity markers (Moreno-Bueno et al., 2008; Kalluri and Weinberg, 2009; Thiery et al., 2009; Kerosuo and Bronner-Fraser, 2012; Lim and Thiery, 2012). Recently, control of epithelial cell–BM interaction has been recognized as another crucial component of EMT regulation (Levayer and Lecuit, 2008; Nakaya et al., 2008; Rowe and Weiss, 2009; Hagedorn and Sherwood, 2011; Williams et al., 2012). However, it is unclear how this regulation is achieved molecularly and whether it utilizes the same signaling and transcriptional mediators as those involved in E-cadherin and apicobasal polarity regulations.

Gastrulation, one of the best-known examples of EMT, is a conserved developmental process during which the three principal germ layers (ectoderm, mesoderm, and endoderm) are generated (Nakaya and Sheng, 2008, 2013; Acloque et al., 2009; Lim and Thiery, 2012; Solnica-Krezel and Sepich, 2012). Gastrulation EMT in amniotes (birds and mammals) involves changes of epiblast cells from a proper epithelium with the full array of epithelial characteristics to mesenchymal-shaped mesoderm cells (Nakaya and Sheng, 2008). The primitive streak, a transient embryonic structure where gastrulation EMT takes place, is composed of cells that have initiated EMT, but are still connected to the rest of the epiblast as a continuous sheet. These cells are considered to be metastable, partial-EMT cells, having

Correspondence to Guojun Sheng: sheng@cdb.riken.jp

The Rockefeller University Press $30.00
J. Cell Biol. Vol. 202 No. 4   637–651
www.jcb.org/cgi/doi/10.1083/jcb.201302075

JCB   637

lost the epiblast cell–BM interaction but retained apicobasal polarity and apical cell–cell junctions. In both chick and mouse models, the first cell-biological sign of gastrulation EMT is the initiation of BM breakdown underneath the epiblast (Nakaya et al., 2008; Williams et al., 2012). We have previously reported that this BM breakdown coincides with and is regulated by the destabilization of microtubules (MTs) at the basal cortex of epiblast cells (Nakaya et al., 2008). Before EMT, MTs in epiblast cells are organized along the apicobasal axis with their plus ends oriented toward the basal cell membrane. In cells undergoing gastrulation EMT, MTs at the basal cell cortex are destabilized, resulting in a weakening of epiblast cell–BM interaction and, consequently, BM breakdown (Nakaya et al., 2008; Nakaya et al., 2011). This process is partially controlled by the loss of basal RhoA activity, but how basal MTs are anchored to the basal cell cortex and how this anchoring regulates the epiblast cell–BM interaction is not well understood.

CLIP-associated proteins (CLASPs) are evolutionarily conserved MT plus end tracking proteins (+TIPs) known to play essential roles in local regulation of MT dynamics (Akhmanova et al., 2001; Carvalho et al., 2003; Akhmanova and Hoogenraad, 2005; Mimori-Kiyosue, 2011). In cultured mammalian cells, CLASPs, together with their binding partners LL5s and other +TIP proteins, mediate the interaction between distal MT ends and the cell cortex (Akhmanova et al., 2001; Lansbergen et al., 2006; Hotta et al., 2010; Mimori-Kiyosue, 2011). But it is unclear whether, during gastrulation EMT, CLASPs are involved in basal cortical anchoring of MTs in epiblast cells; and if so, how CLASPs can facilitate cross-interaction between the cytoskeleton and the BM. One potential candidate for mediating such cross-interaction is Dystroglycan (DG). DG was isolated as a component of the dystrophin–glycoprotein complex and functions by connecting muscle BM, sarcolemma, and muscle cytoskeleton (Ervasti and Campbell, 1991; Ibraghimov-Beskrovnaya et al., 1992). DG is composed of α and β subunits encoded from a single *dystroglycan* (*DAG1*) gene. α-DG is localized extracellularly and binds to laminin and other BM components; and β-DG is a transmembrane protein that interacts extracellularly with α-DG and intracellularly with actin filaments and MTs (Campbell, 1995; Henry and Campbell, 1999; Ayalon et al., 2008; Cerecedo et al., 2008; Bozzi et al., 2009; Prins et al., 2009).

In this paper, we investigated the role of CLASPs in basal MT stabilization and cortical anchoring during avian gastrulation EMT. We also analyzed the involvement of DG in linking the intracellular cortical MTs with the extracellular BM. We show that CLASPs and their binding partners LL5s stabilize MTs in the basal cortex. Overexpression of CLASPs in streak epiblast cells results in BM retention, and CLASP mutants lacking the MT and cortical binding ability or antisense morpholino (MO)-mediated knockdown of CLASPs and LL5s lead to premature BM breakdown in lateral epiblast cells. Furthermore, we provide evidence that CLASPs regulate basal membrane localization of DG, and that this localization is required for stabilizing the basal membrane–BM interaction in pre-EMT epiblast cells. Disengagement of this stabilizing mechanism promotes BM breakdown and initiates gastrulation EMT.

Results

CLASP mRNAs are expressed in chicken epiblast cells during gastrulation

Like in mammals, there are two CLASP genes in the chicken genome, *CLASP1* (available from GenBank under accession no. XM_426599) and *CLASP2* (accession no. NM_001177385). Sequence alignment analysis (Fig. S1 A) revealed that chicken *CLASP1* and *CLASP2* are orthologous to human *CLASP1* (accession no. NP_056097) and *CLASP2* (NP_055912), respectively. Three TOG (tumor overexpressed gene) domains and regions for EB1, CLIP, and LL5 binding are highly conserved. To see whether chicken CLASP genes are expressed during gastrulation, we generated antisense RNA probes (Materials and methods) and analyzed their mRNA expression patterns. The *CLASP1* gene starts to be expressed before streak formation (HH1 in Fig. 1 A). Strong expression was detected at gastrulation stages in the area pellucida, and at later stages the expression became limited to the neural territory (HH3–4 in Fig. 1 A and HH5–7 in Fig. S1 B). Section analysis revealed that *CLASP1* expression at stage HH4 was restricted to the epiblast (Fig. 1 A1). Medial epiblast cells within the streak exhibited down-regulated *CLASP1* levels, and mesoderm cells showed very weak or no expression (Fig. 1 A1). Expression of *CLASP2* mRNAs was relatively weaker than that of *CLASP1*, but these two genes had very similar dynamic patterns (Fig. 1 B and Fig. S1 C). At stage HH4, *CLASP2* expression was likewise detected in the epiblast, down-regulated in medial epiblast cells, and absent in the mesoderm (Fig. 1 B1). These results suggested that both CLASP genes function in chicken epiblast cells before they undergo gastrulation EMT.

CLASPs function to maintain BM integrity through their MT-binding ability during EMT

It has been reported that CLASPs can mediate the interaction between the cell cortex and MT plus ends in mammalian culture cells and that CLASPs together with their binding partners LL5s mediate cellular interaction with laminin-based cell substrate (Mimori-Kiyosue et al., 2005; Hotta et al., 2010). We asked whether chicken CLASPs play a role in epiblast cell–substrate interaction before and during gastrulation EMT. First, we electroporated constructs either expressing control enhanced GFP (eGFP) or expressing eGFP-CLASP1α or eGFP-CLASP2γ (eGFP-tagged human CLASP1α or human CLASP2γ, respectively; Akhmanova et al., 2001; Mimori-Kiyosue et al., 2005) into lateral epiblast cells at the mid-streak level of stage HH3–4 embryos. CLASP1α is the full-length isoform of CLASP1, and CLASP2γ is a short splicing isoform of CLASP2 with full MT binding efficiency. Electroporated embryos were incubated for another 6–7 h followed by fixation and staining for laminin expression. In control embryos, eGFP-expressing cells ingressed normally and became mesoderm cells (Fig. 1 C, top). The BM underneath medial epiblast cells at the primitive streak (both eGFP-positive and -negative cells) was properly broken down (Fig. 1 C) as in normal untreated embryos (Nakaya et al., 2008). In contrast, the BM underneath medial epiblast cells
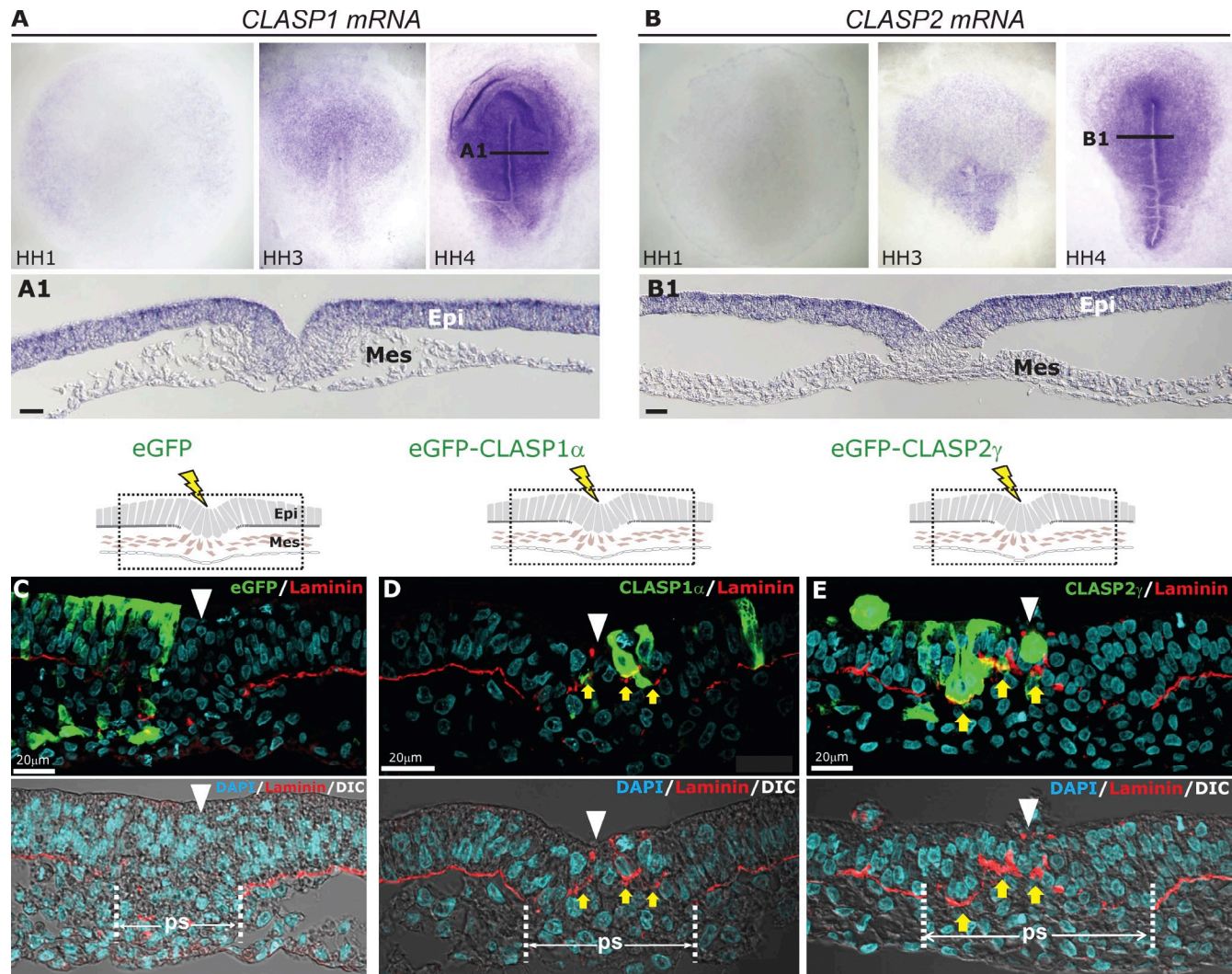
Figure 1.   **Endogenous CLASP mRNA expression and the effect of exogenous CLASP overexpression on laminin in the primitive streak.** (A and B) Whole-mount in situ hybridization of *CLASP1* (A) and *CLASP2* (B) transcripts. Both *CLASP1* and *CLASP2* are expressed in epiblast cells (epi) and absent in mesoderm cells (mes). Bars, 20 µm. (C–E) Effect of CLASP overexpression on laminin. (C) eGFP control overexpression. Normal laminin breakdown and normal ingression of expressing cells. (D and E) Electroporation with eGFP-CLASP1α (D) or eGFP-CLASP2γ (E) expression vectors. Arrowheads, streak midline; yellow arrows, laminin retention in CLASP-expressing cells. ps, primitive streak. Bars, 20 µm.

expressing eGFP-CLASP1α or eGFP-CLASP2γ remained to be laminin positive (Fig. 1, D and E, arrows), which suggested that endogenous CLASPs function to maintain BM integrity during gastrulation.

Previous studies showed that MT plus end and cortical binding ability of CLASPs are necessary for MT stabilization in the leading edge of fibroblast cells (Akhmanova et al., 2001; Mimori-Kiyosue et al., 2005). We next examined whether MT plus end and cortical binding of CLASP2 is involved in laminin retention in primitive streak cells. The CLASP2-ΔMΔC mutant has its EB1-binding domain in the middle and CLIP-binding domain in the C terminus deleted (Fig. 2 A), and lacks the MT plus end binding activity in COS cells (Akhmanova et al., 2001; Mimori-Kiyosue et al., 2005). No laminin retention was observed when eGFP-CLASP2-ΔMΔC mutant was expressed in the primitive streak (Fig. 2 B, arrows), which suggests that the laminin retention phenotype seen with eGFP-CLASP2γ

requires the MT plus end and cortical binding ability of CLASP2. Interestingly, we saw ectopic laminin breakdown when eGFP-CLASP2-ΔMΔC was expressed in lateral epiblast cells where laminin should be present (arrows in Fig. 2 C and control in Fig. 2 D and Fig. S2 A). A similar effect in lateral epiblast cells was also seen with CLASP2-ΔC, a CLASP2 mutant with the C-terminal domain deleted (Fig. 2, A and D; and Fig. S2 B). CLASP2-ΔM, a CLASP2 mutant with the EB1 binding domain deleted, caused only a very mild disruption of laminin expression in the lateral epiblast cells (Fig. 2, A and D; and Fig. S2 C). These results suggest that the C-terminal domain is important for laminin maintenance in lateral epiblast cells before EMT. To confirm the involvement of CLASPs in mediating the cell–BM interaction in lateral epiblast cells, we used specific antisense MOs to knock down endogenous levels of CLASPs. Although CLASP2 MOs showed only a weak phenotype (Fig. 2 G), CLASP1 MOs caused potent laminin breakdown
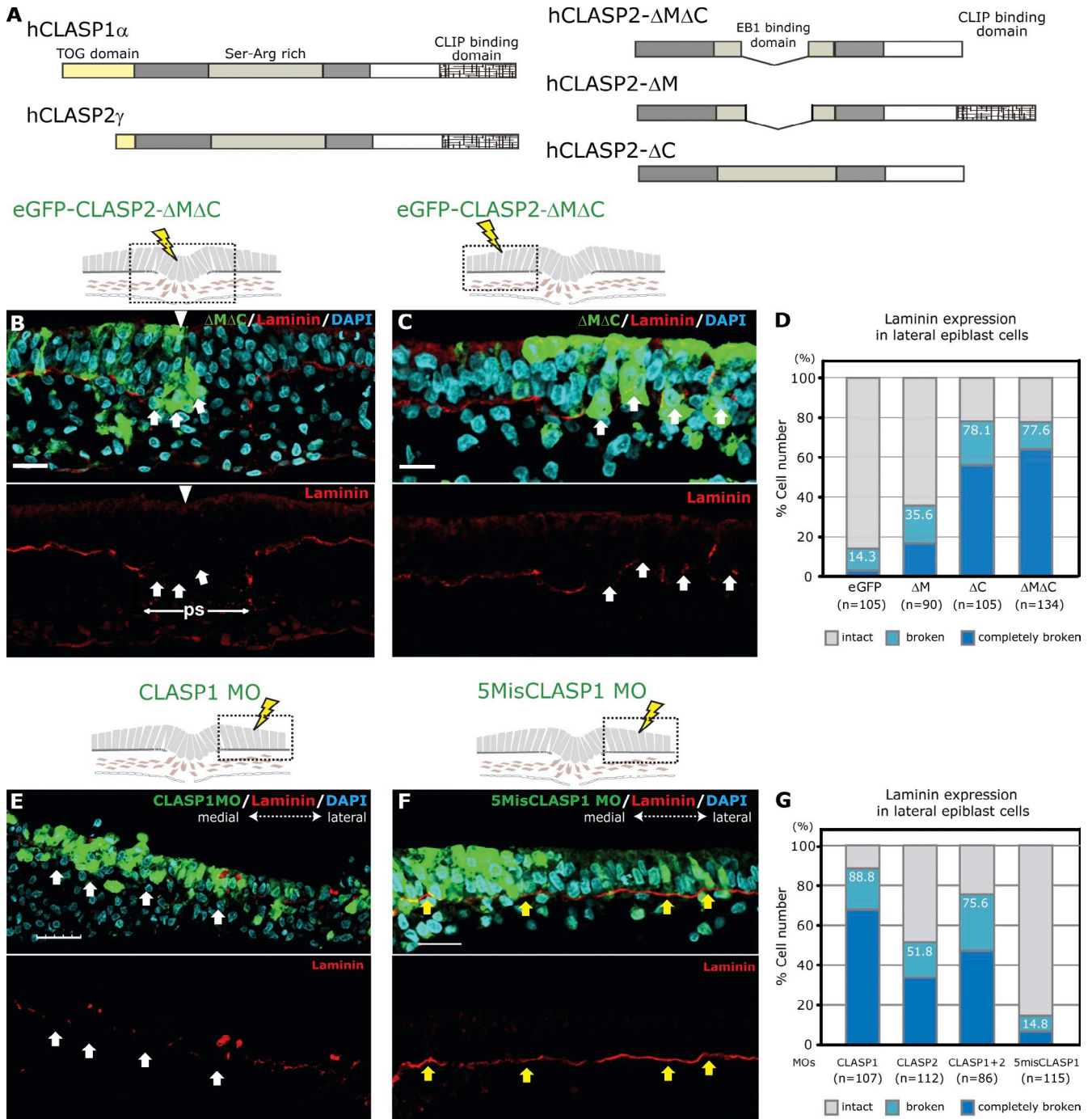
Figure 2. **CLASPs maintain BM integrity during EMT through their MT-binding ability.** (A) Schematic diagram of human CLASP1α and human CLASP2γ, and deletion mutants of human CLASP2 used in this study. (B and C) Effect of eGFP-CLASP2-ΔMΔC overexpression. White arrowheads in B indicate the streak midline. White arrows in B indicate normal BM breakdown in streak midline cells. White arrows in C indicate that CLASP2-ΔMΔC–overexpressing cells in lateral epiblast region have premature laminin breakdown. (D) Percentage of expressing cells showing laminin breakdown. Phenotypes are classified into three categories: no breakdown, mild breakdown, and complete breakdown. ΔMΔC (77.6%, n = 134 cells from six embryos) and ΔC (78.1%, n = 105 cells from four embryos) showed severe phenotypes. ΔM mutant showed a mild phenotype (35.6%, n = 90 cells from four embryos) in comparison with control GFP (14.3%, n = 105 cells from five embryos). (E) Knockdown of CLASP1 protein by CLASP1-specific MOs caused laminin breakdown. White arrows indicate ectopic BM breakdown in lateral epiblast cells. (F) 5mis-control MO does not affect laminin expression. Yellow arrows indicate normal BM levels in 5mis-CLASP1 control MO–receiving cells. (G) Percentage of MO-containing cells showing laminin breakdown with different MOs. CLASP1 MO, 88.8% (n = 107 cells from five embryos); CLASP2 MO, 51.8% (n = 112 cells from three embryos); CLASP1 + CLASP2 MOs, 75.6% (n = 86 from three embryos); 5mis CLASP1 control MO, 14.8% (n = 115 from three embryos). Bars, 20 µm.

in lateral epiblast cells (Fig. 2, E and G, arrows). 5-mis control of CLASP1 MOs had no effect on laminin expression (Fig. 2, F and G). These data suggested that maintenance of the cell–BM

interaction in chicken epiblast cells requires the C-terminal domain of CLASP proteins, and that CLASP down-regulation leads to BM breakdown during gastrulation EMT.
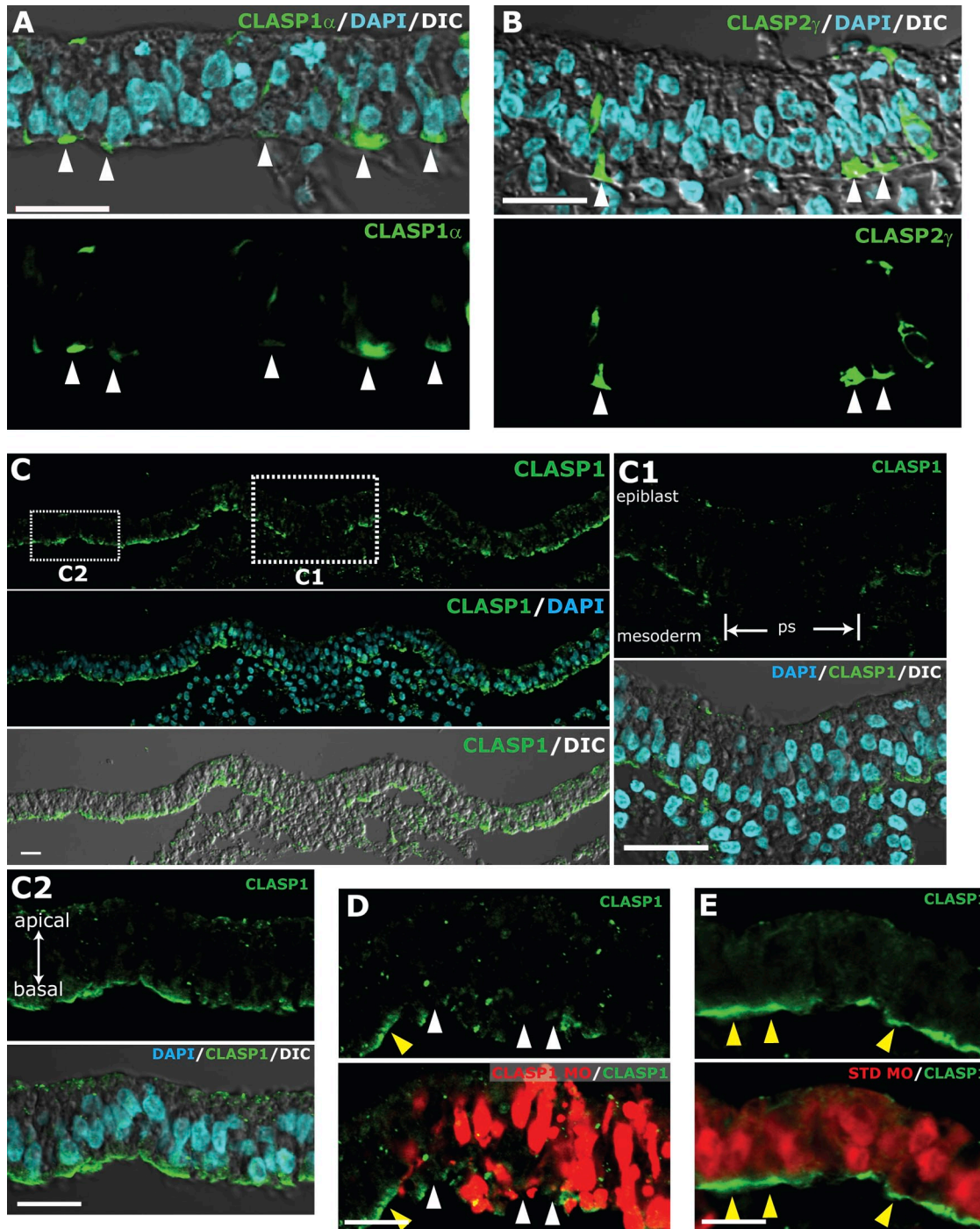
Figure 3. **CLASP proteins are localized to the basal cortex in lateral epiblast cells.** (A and B) When eGFP-CLASP1α (A) or eGFP-CLASP2γ (B) is electropor-ated into lateral epiblast cells at low concentrations, GFP signals are detected at the basal side. Arrowheads indicate basal localization of CLASP1α (A) and CLASP2γ (B). (C) Endogenous CLASP protein signals detected by cCLASP1 antibody are localized to the basal side. ps, primitive streak. (D and E) Valida-tion of cCLASP1 antibody specificity. In standard MO-electroporated cells (E, yellow arrowheads), basal cCLASP1 antibody signals are not diminished. In CLASP1 MO–electroporated cells, basal cCLASP1 antibody signals are diminished. Yellow arrowheads in D show the normal level of cCLASP1 signals in cells not receiving CLASP1 MO. White arrowheads indicate loss of basal CLASP1 in CLASP1 MO receiving cells. Bars, 20 μm.

CLASP proteins are localized to the basal side of lateral epiblast cells before EMT

We next asked whether subcellular localization of chicken CLASPs is consistent with their putative role in mediating epi-blast cell–BM interaction. When low concentrations of either eGFP-CLASP1α– or CLASP2γ-expressing constructs were introduced into lateral epiblast cells, both were found to be local-ized mainly to the basal side (Fig. 3, A and B, arrowheads). To investigate endogenous CLASPs' subcellular localization, we generated antibodies against the chicken CLASP1 (cCLASP1 antibody), which was produced using a polypeptide corre-sponding to amino acid residues 189–325 of chicken CLASP1.

Figure 4. **CLASPs and LL5s cooperate in maintaining BM integrity in lateral epiblast cells.** (A and C) Electroporated at low concentrations, eGFP-LL5α (A) and eGFP-LL5β(C) have a basal cortical localization (white arrows). (B and D) Overexpression of eGFP-LL5α (B) and eGFP-LL5β (D) in streak cells causes ectopic laminin expression (yellow arrows). ps, primitive streak. (E) Quantification of laminin breakdown when LL5s or LL5s + CLASP1 are knocked down with MOs in lateral epiblast cells. LL5 and CLASP1 knockdown leads to strong laminin breakdown phenotypes. (F–I) Examples of phenotypes caused by LL5α and β double MO (F), LL5α (G), or LL5β (H) single MO, standard control MO (I), and LL5 and CLASP1 triple MO (J) knockdown. White arrows in F–H and J indicate premature BM breakdown. Yellow arrows in I indicate normal BM in standard MO-receiving cells. Arrowheads indicate the streak midline. Bars, 20 μm.
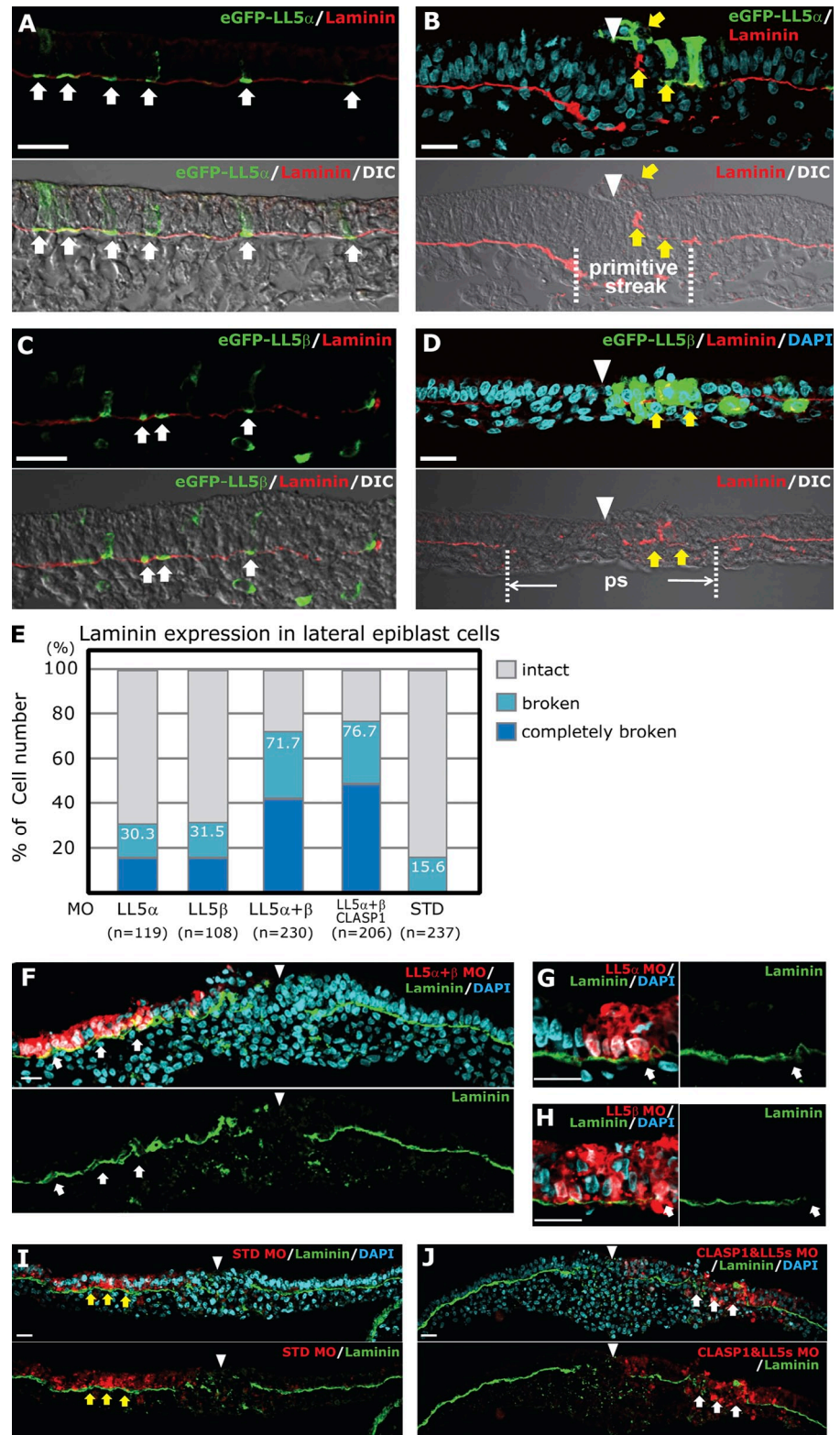
Immunohistochemistry analysis showed that the cCLASP1 antibody signals were localized to the basal side of lateral epiblast cells (Fig. 3 C, C2), and no signal was observed on the basal side in medial epiblast cells (Fig. 3 C, C1). We next validated the specificity of cCLASP1 antiserum using CLASP1 MO. In lateral epiblast cells expressing CLASP1 MO, cCLASP1 antibody signals were reduced prominently (Fig. 3 D, white arrowheads), whereas standard MO-receiving cells showed no change in CLASP1 basal expression (Fig. 3 E, yellow arrowheads). These observations are consistent with our hypothesis that basally localized CLASP proteins contribute to lateral epiblast cell–BM interactions and that dissociation of CLASPs from the basal cortex in medial streak cells contributes to BM breakdown during gastrulation EMT.
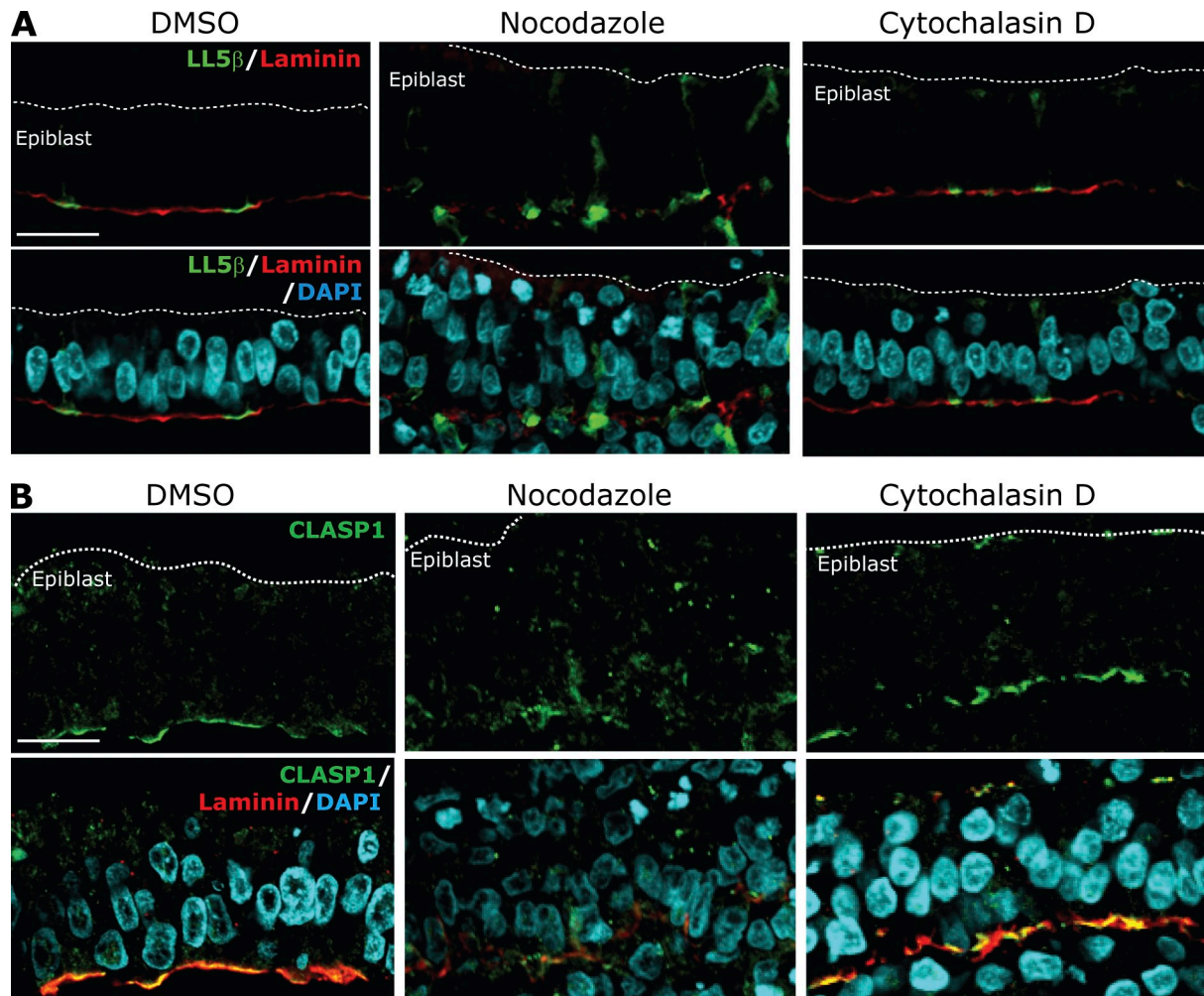
Figure 5. **Localization of LL5β and CLASP1 after nocodazole and cytochalasin D treatment.** (A) eGFP-LL5β localization after control DMSO (left), nocodazole (middle), and cytochalasin D treatment for 2 h. (B) Endogenous CLASP1 localization after control DMSO (left), nocodazole (middle), and cytochalasin D treatment for 1.5 h. Broken lines indicate the apical limit of the epiblast. Bars, 20 μm.

LL5s play an inter-linking role with CLASPs in the basal cortex of epiblast cells to maintain BM integrity

It has been reported that LL5α and -β, also known as pleckstrin homology (PH)-like domain family B member 1 and 2 (PHLDB1 and -2), respectively, are localized adjacent to laminin-5 deposition in mammary epithelial cells (Hotta et al., 2010). Functionally, LL5α and -β are CLASP binding partners, and it has been hypothesized that CLASP–LL5 complex anchors MT plus ends to the site where deposited laminin interacts with its receptor integrins (Hotta et al., 2010; Mimori-Kiyosue, 2011). In chicken gastrula, transcripts of both *LL5α* and *LL5β* were detected in epiblast cells (Fig. S3). We first investigated subcellular localization of LL5s in lateral epiblast cells and found that when either eGFP-LL5α or eGFP-LL5β was expressed, they were predominantly localized to the basal cortex (Fig. 4, A and C, arrows). Interestingly, when high concentrations of the LL5α or LL5β gene were overexpressed, we observed laminin retention in streak cells, a phenotype similar to that of CLASP overexpression (arrows in Fig. 4, B and D). When LL5α and -β were simultaneously knocked down in lateral epiblast cells, premature BM breakdown was observed (71.7% with *n* = 230 cells; Fig. 4, E and F), whereas MOs against either LL5α (30.3% with *n* = 119 cells; Fig. 4, E and G) or LL5β (31.5% with *n* = 108 cells; Fig. 4, E and H) had a weaker, but still detectable effect. The combination of anti-LL5 and anti-CLASP1 MOs also resulted in a clear effect on laminin expression (76.7%, *n* = 206 cells; vs. control 15.6%, *n* = 237 cells; Fig. 4, E, I, and J). The severity caused by triple MOs (LL5s and CLASP1) was however slightly less than that by single CLASP1-MO knockdown (88.8% in Fig. 2 G), possibly due to dilution of MO concentrations in triple mix. We next asked whether subcellular localization of LL5s depends on cortical MT stability. When embryos were treated with nocodazole, an MT-disrupting drug, the basal cortical localization of LL5β was only mildly affected (Fig. 5 A, middle), although nocodazole's effect on basal MT dynamics was strong as revealed by acetylated tubulin and laminin staining (Fig. S4, A and B). Control DMSO or cytochalasin D treatment did not affect LL5β localization (Fig. 5 A, left and right panels, respectively). In contrast, CLASP1 protein became diffuse and localized away from the basal cortex after nocodazole treatment (Fig. 5 B). In LL5 MO cells, basal cortical localization

of CLASP1 was only mildly affected (Fig. S4 C). These results indicated that LL5α and β are localized to the basal cortex in an MT-independent fashion. Their interaction with CLASPs could help stabilize basal MTs and maintain the integrity of extracellular laminin in lateral epiblast cells.

CLASPs and LL5s are required for anchoring MTs to the basal cell cortex in lateral epiblast cells

We therefore examined whether CLASPs and LL5s can stabilize and anchor MTs to the basal cortex in lateral epiblast cells. For this purpose we performed live epiblast cell imaging of EB1 comets, which mark the growing MT plus ends (Fig. 6 A). Time-lapse movie sequences (1 s per frame for 1 min) of GFP-fused EB1-expressing epiblast cells were acquired by using spinning-disk confocal microscopy. When images were taken from the apical side, EB1 fluorescence signals at the apical cortex were strong and could be observed to move toward the lateral rims of the cell in a radial fashion (Fig. 6 B and Video 1, taken from the apical side). But signals from the basal cortex were very weak. We therefore decided to image from the basal side after physical removal of mesoderm and endoderm tissues. With this method we were able to visualize EB1 comets at both apical and basal cortices of epiblast cells (Fig. 6 A). We attempted to analyze EB1 comets in CLASP1 MO–receiving cells. However, maximal concentration of CLASP1 MO led to severe defects in epithelial polarity (Fig. 2 E), which was not an appropriate condition for tracking EB1 dynamics. When we reduced the concentration of CLASP1 MO so that the epithelial polarity was maintained, no obvious difference was seen between control MO– and CLASP1 MO–treated cells. However, when we adjusted the triple MO (CLASP1 and LL5s) concentrations, a reduction in basal MT dynamics in triple MO receiving was observed compared with control MO–receiving cells. In control MO–treated cells, the movement of EB1 comets at the basal side was not as dynamic as that at the apical side, but was still readily detectable (Fig. 6 C, top; and Video 2). This is in agreement with the presence of MTs at the basal cell cortex, which we had reported previously using electron microscopy and biochemical methods (Nakaya et al., 2008). In contrast, when CLASP1 and LL5s were knocked down, EB1 signals were reduced at the basal side (Fig. 6 C, bottom; and Video 3). The difference between these two types of cells in MT distribution was also seen in 3D-reconstituted images (compare the top-right panel in Fig. 6 C and Videos 4 and 5 with the bottom-right panel in Fig. 6 C and Videos 6 and 7). This suggested that MTs in the basal region were destabilized in triple MO–receiving cells that had a broken BM (Fig. S4 D) and reduced levels of basal CLASP1 (Fig. S4 D) and basal MT (Fig. S5, A and B). Quantification analysis of basal EB1-GFP signals relative to total EB1-GFP signals (Fig. 6 E) in control MO cells versus triple MO cells exhibiting mild phenotypes, in which measurement of basal EB1-GFP signals was still possible (Fig. 6 D), supported this hypothesis (Fig. 6, F and G). Collectively, although the epistatic relationship between MT stability and cortical localization of CLASPs/LL5s awaits further clarification, these data suggested that they mutually reinforce each other, and together they regulate the epiblast cell–BM interaction.

DG plays a role in mediating the BM–basal cell interaction during EMT

How can the intracellular interplay between MTs, CLASPs, and LL5s promote cell–BM interactions and extracellular BM integrity? Bioinformatics data mining of our primitive streak transcriptomic analyses (Alev et al., 2010; Nakaya et al., 2011) suggested two categories of genes, encoding transmembrane proteins—integrins and DGs, respectively—as potential mediators. Integrins, through adaptor proteins such as talin and α-actinin, are known to mediate extracellular matrix and intracellular F-actin interaction. Their role in MT-mediated cell–BM interaction is less clear. We have previously shown that integrins are expressed and likely play a role in gastrulation EMT (Nakaya et al., 2008). But the presence of multiple α and β integrin genes in the primitive streak makes functional analysis difficult. DG, however, is known to interact with both the F-actin and MTs, and its two subunits, α-DG and β-DG, are encoded by a single *DAG1* gene. In this work, we focused our investigation on DG as a potential link between the BM and cortically stabilized MTs. During gastrulation, DG expression is restricted to the epiblast cells (Nakaya et al., 2011). Subcellularly, DG is localized to the basolateral membrane in lateral epiblast cells; and in streak epiblast cells, basal membrane localization of DG is lost and lateral membrane localization is weakly detectable (Fig. 7 A). When wild-type DG was overexpressed in streak epiblast cells, laminin retention was observed (Fig. 7 C, arrows; with control shown in Fig. 7 B). Knockdown of DG in lateral epiblast cells with MOs resulted in abnormalities in cell shape and BM integrity (Fig. 7, D–F). In contrast to control MOs, cells receiving translation blocking type MO (TB) or TB + splicing blocking type MO (TB+SB) showed premature breakdown of laminin (TB−MO, 81.7% with n = 149 cells; TB+SB−MOs, 74.5% with n = 153 cells; Fig. 7, D and E, arrows; and Fig. 7 F). Overall, these results indicated that basally localized DG plays a role in mediating the epiblast cell–BM interaction during EMT.

CLASP affects basal DG localization during EMT

We next investigated whether there is a functional relationship between CLASPs and DG. In normal epiblast cells, β-DG is localized to the basolateral cell membrane. The basal membrane domain has relatively stronger expression than the lateral one (Fig. 7 A). Knockdown of CLASP levels in lateral epiblast cells led to a reduction in basal β-DG expression (Fig. 8, A and E). In contrast, 5mis-CLASP1-MOs (Fig. 8, D and E) or LL5 MOs (Fig. S5 C) had no effect on the subcellular localization of β-DG in lateral epiblast cells. A similar effect on β-DG localization was observed when the dominant-negative eGFP-CLASP2-ΔMΔC was electroporated (Fig. 8, B, C, and E), and wild-type eGFP-CLASP2γ overexpressing medial streak cells retained strong DG expression (Fig. 8 F, arrows). These results strongly suggested that CLASPs regulate basal DG localization in epiblast cells before EMT. We asked whether there is a physical interaction between CLASPs and DG. HEK293T cell lysates of either CLASP or control transfectants were examined for coimmunoprecipitation of cotransfected β-DG. We found that anti–β-DG
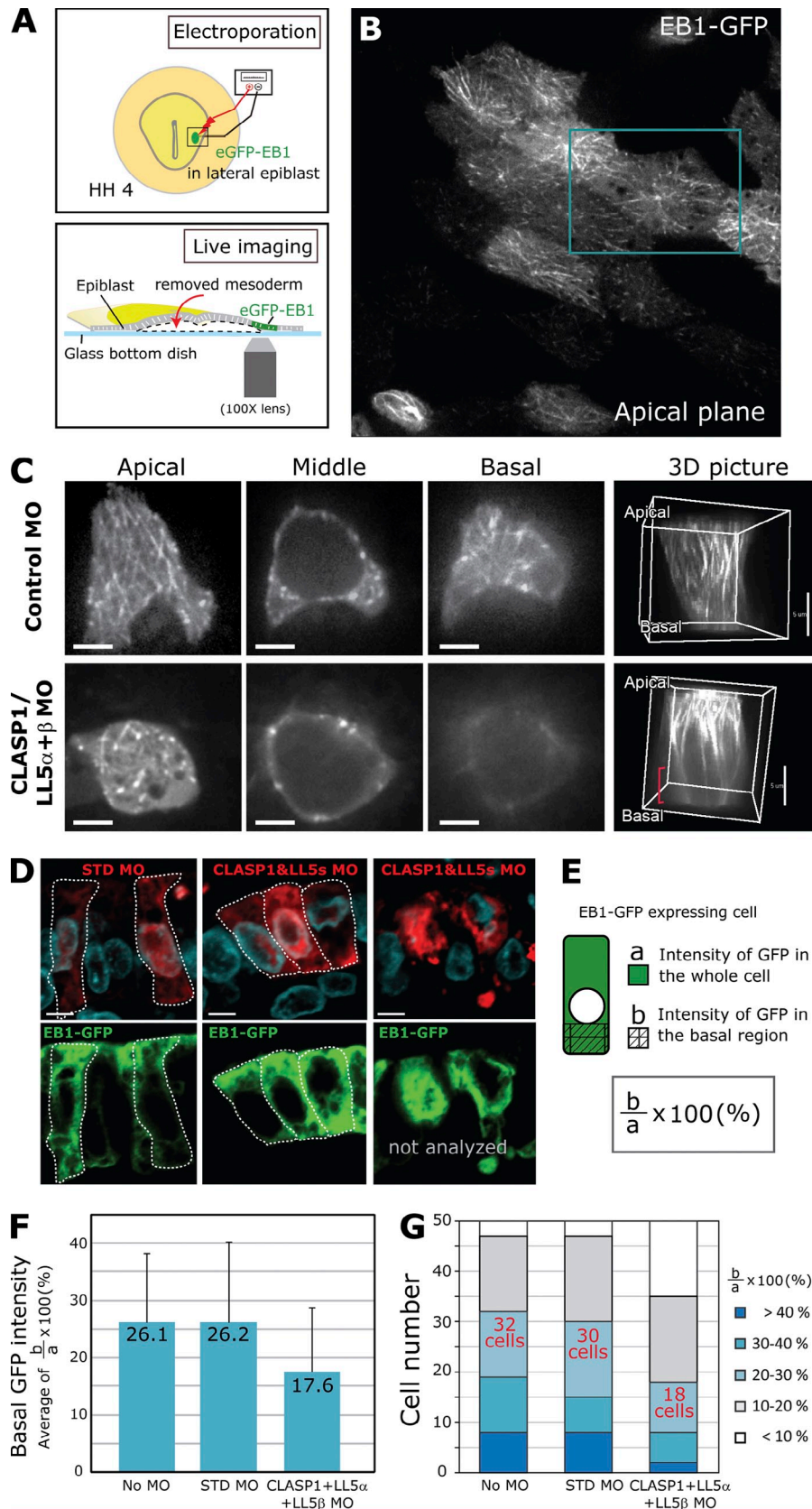
Figure 6. **CLASP and LL5s are involved in regulating basal MT dynamics.** (A) Diagram of eGFP-EB1 electroporation and live-embryo imaging. (B) Imaging of lateral epiblast cells from the apical side. eGFP-EB1 molecules show dynamic and radial movement from the center toward the rim of the cell. (C) Imaging of lateral epiblast cells from the basal side. EB1 signals in the apical, middle, and basal planes in control MO cell (top) or CLASP1 and LL5s MO cell (bottom). In the latter cell, EB1 signals are relatively weaker basally. Right-most panels are examples of 3D-reconstituted images showing the difference in eGFP-EB1 signals between control and CLASP/LL5s knockdown cells. (D–F) Quantification of relative basal eGFP-EB1 signal intensity in frozen sections. (D) Examples of cellular morphology with electroporated control MOs (left) and triple MOs (middle, mild phenotype; right, severe phenotype). Only triple MO cells with mild phenotype are used in quantification. Broken lines outline individual epiblast cells. (E) Relative eGFP-EB1 intensity is calculated as a ratio between basal cortical signals and total cellular signals. (F) Mean relative basal eGFP-EB1 signal intensity in cells ($n = 50$) without MO, with standard MO, or with triple knockdown MOs. (G) Relative intensities are shown as proportions of cells with their basal eGFP-EB1 signals representing the 10th, 20th, 30th, and 40th percentiles of total eGFP-EB1 signals. Error bars indicate one standard deviation. Bars, 5 µm.

antibody can coprecipitate with either HA-CLASP1α or HA-CLASP2γ, and that anti-HA antibody can also coprecipitate with β-DG (Fig. 8 G). Results from proximity ligation assays (Fig. 9, A–E) further supported the idea that there is a physical association between the CLASPs and DG in epiblast cells undergoing gastrulation EMT.
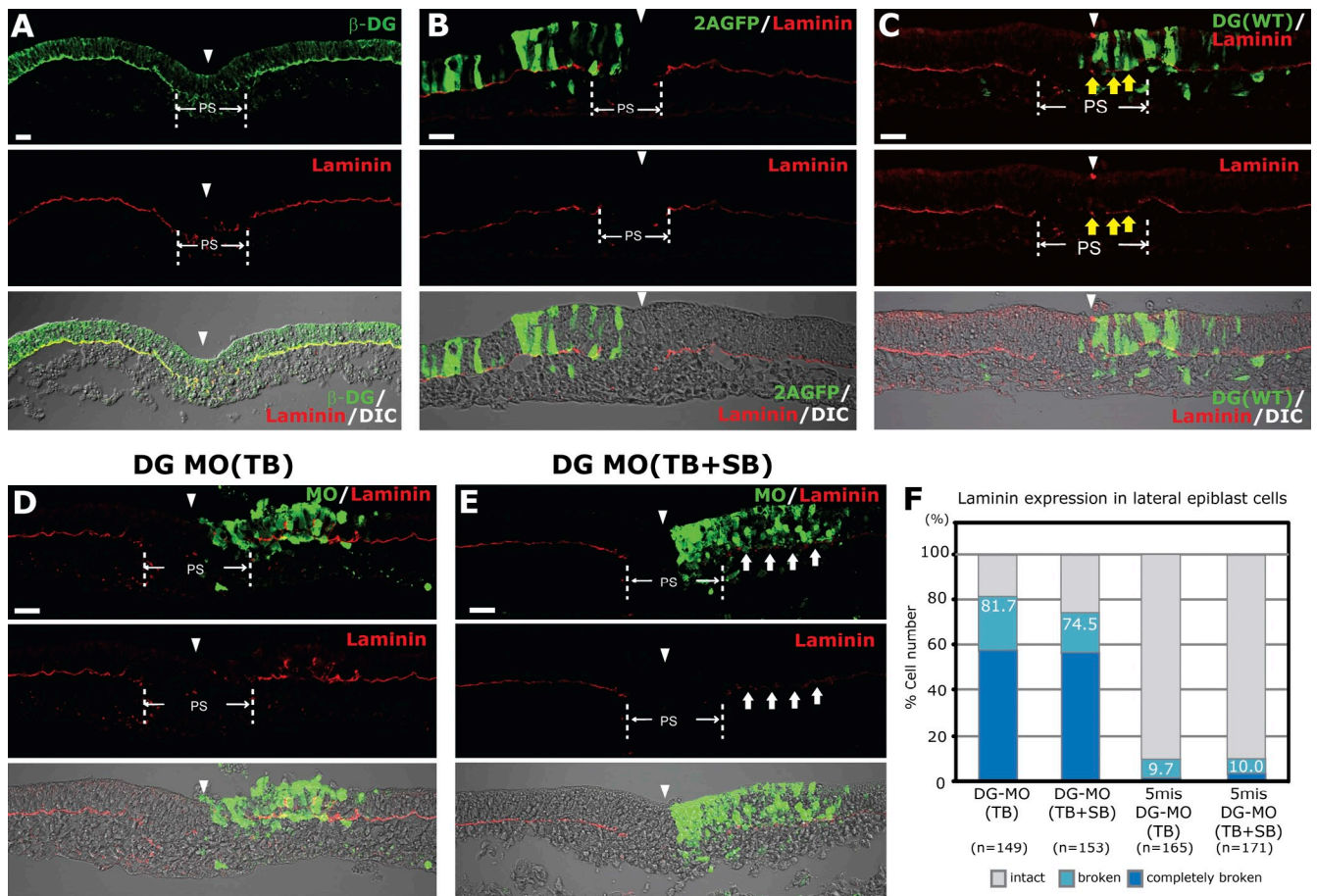
Figure 7. **DG mediates basal membrane–BM interaction in epiblast cells.** (A) β-DG localization in epiblast cells. (B and C) Electroporation with control 2A-eGFP or wild-type (WT)-DG-2A-eGFP expression vector. No obvious change in laminin expression is observed in control 2A-eGFP–expressing cells (B). WT-DG–receiving cells (C) show ectopic laminin expression (yellow arrows). (D and E) DG-specific MOs cause premature laminin breakdown (white arrows). (D) Translation blocking (TB) MO. (E) TB-MO + splicing blocking (SB) MO. ps, primitive streak. Arrowheads indicate the streak midline. (F) Percentage of cells showing laminin breakdown. TB-MO cells: 81.7%, n = 149 cells. TB-MO + SB-MO cells: 74.5%, n = 153 cells. 5-mis TB-MO: 9.7%, n = 165. 5mis TB-MO + SB-MO cells: 10.0%, n = 171. Bars, 20 µm.

Discussion

EMT involves dissociation of cell–cell and cell–matrix interactions in very different physiological and pathological contexts. In many epithelia, apicobasal MT arrays important for generating epithelial polarity are anchored to the basal cortex, where they also play a role in maintaining the epithelial cell–BM interaction (Bacallao et al., 1989; Müsch, 2004; Nakaya et al., 2008; Hotta et al., 2010). Using gastrulation EMT as a model, this work demonstrated that before epiblast cells initiate EMT, MT +TIP proteins CLASP1 and CLASP2, and their binding partners LL5s, regulate MT anchoring to the basal cortex (Fig. 10). Furthermore, we identified DG as a molecular link between the intracellular cortical MTs and extracellular BM, with its membrane-spanning β subunit interacting with cortical CLASPs (Fig. 10).

In our CLASP mutant analysis, overexpression of either ΔC or ΔMΔC mutant caused an ectopic breakdown of laminin in lateral epiblast cells where BM should be intact (Fig. 2, C and D; and Fig. S2 B), which suggests that the C-terminal region of CLASP is important to maintain the BM integrity. This region in human CLASP2 was shown to interact with CLIP-170

and CLIP-115 (Akhmanova et al., 2001), as well as LL5 (Mimori-Kiyosue et al., 2005). The same region in human CLASP1 was reported to mediate CLASP dimerization, and its deletion resulted in a dominant-negative phenotype on MT polymerization (Patel et al., 2012). Cls1p, the *Schizosaccharomyces pombe* CLASP, also uses this region for dimerization (Al-Bassam et al., 2010). It is therefore likely that the phenotype we observed with C-terminal deletion mutants was caused by a disruption of monomer/dimer balance of CLASPs or the binding with their partners such as LL5s, or both.

Our previous work (Nakaya et al., 2008) indicated that the cortically enriched small GTPase RhoA's activity plays a critical role in stabilizing MTs anchored at the basal cell cortex during gastrulation EMT. We have yet to investigate whether and how RhoA activity modulates DG-CLASPs–LL5s-MT interactions. Rho GTPases are activated by guanine nucleotide exchange factors (GEFs) that catalyze GTP loading. Net1, a RhoA-specific GEF, is expressed in epiblast cells and can regulate RhoA activity at the basal cortex (Nakaya et al., 2008). Inactive Net1 protein is sequestered in the nucleus, and its basal cortical localization when activated has been proposed to be
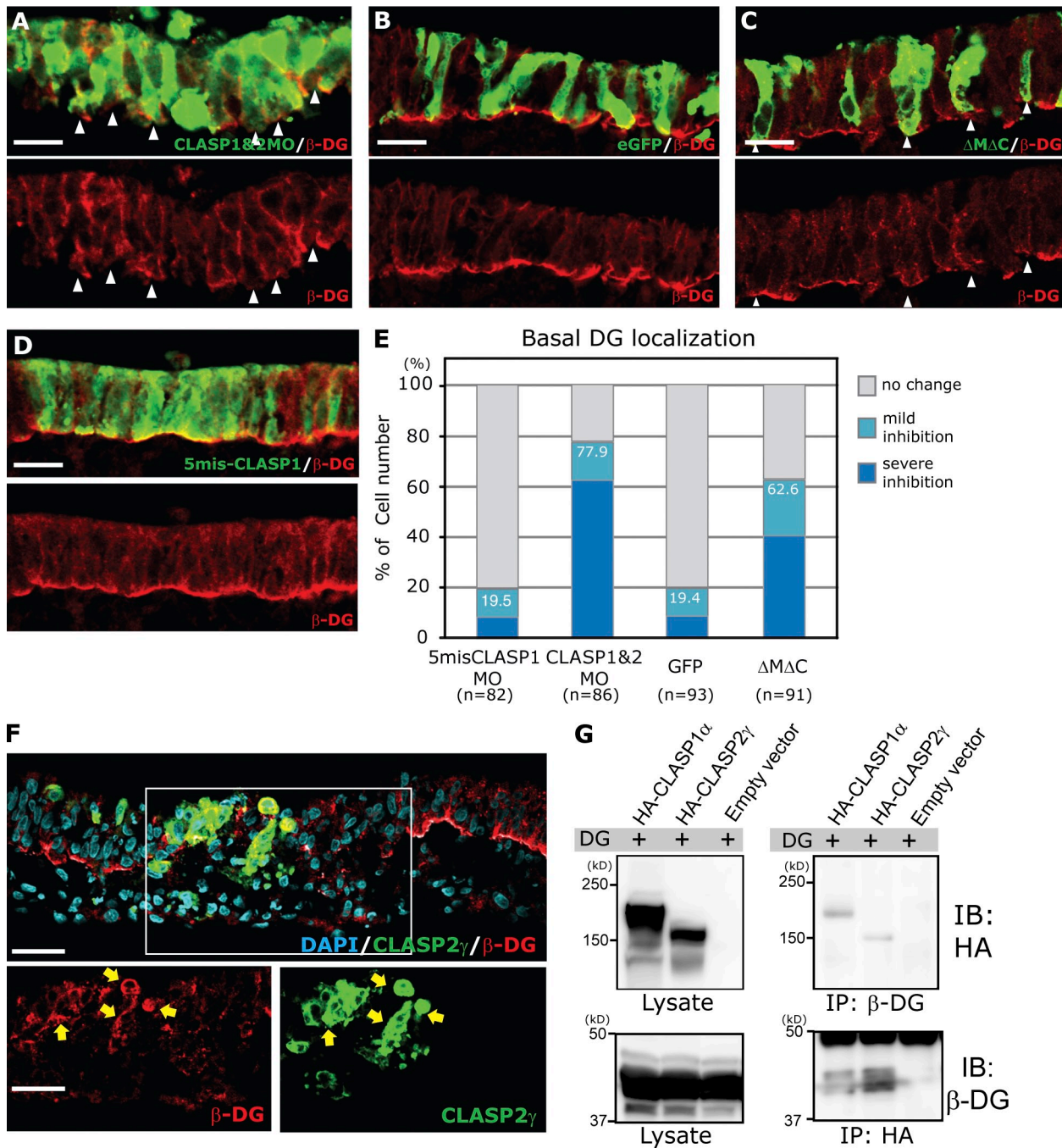
Figure 8. **CLASP affects basal DG localization during EMT.** (A) CLASP1 + CLASP2 MOs reduce basal DG localization. (B) Standard control MO does not affect DG subcellular localization. (C) CLASP2-ΔMΔC reduces basal DG localization. (D) 5mis-CLASP1 MO–expressing cells show no change in DG local-ization. Arrowheads indicate reduction of basal DG localization. (E) Percentage of cells showing a reduction in basal DG. CLASP1 + CLASP2 MOs cells: 77.9%, n = 86 cells from five embryos. 5mis CLASP1 control MO cells: 19.5%, n = 82 cells from three embryos. eGFP-expressing control cells: 19.4%, n = 93 cells from three embryos. eGFP-ΔMΔC expressing cells: 62.6%, n = 91 cells from four embryos. (F) eGFP-CLASP2γ–expressing cells retain strong DG expression in the medial streak. Arrows indicate mislocalization of DG in CLASP2γ–expressing cells. (G) Immunoprecipitation with either anti–β-DG anti-bodies or anti-HA antibodies from HEK 293 cells transfected with human DG and either HA-CLASP1α, HA-CLASP2γ, or mock treatment. Bars, 20 µm.

under the regulation of MTs extending to the basal cortex (Schmidt and Hall, 2002; Nakaya et al., 2008). Although fur-ther evidence is needed, a possible scenario is that CLASPs–LL5s-MT interactions regulate basally targeted growth of MTs and transport of Net1, resulting in basally enriched RhoA acti-vation. Our preliminary data suggested that RhoA overexpres-sion affects endogenous DG localization in streak cells, and

we showed in this work that β-DG can be coprecipitated with CLASPs in vitro (Fig. 8 G) and interacts with CLASPs in vivo (Fig. 9). It is therefore likely that in a positive feedback loop, RhoA activity controls basal cortical MT dynamics by influencing interactions among components of the DG-CLASPs–LL5s-MT complex, as has been implicated by its ability to positively regu-late +TIPs EB1 and APC (Wen et al., 2004).
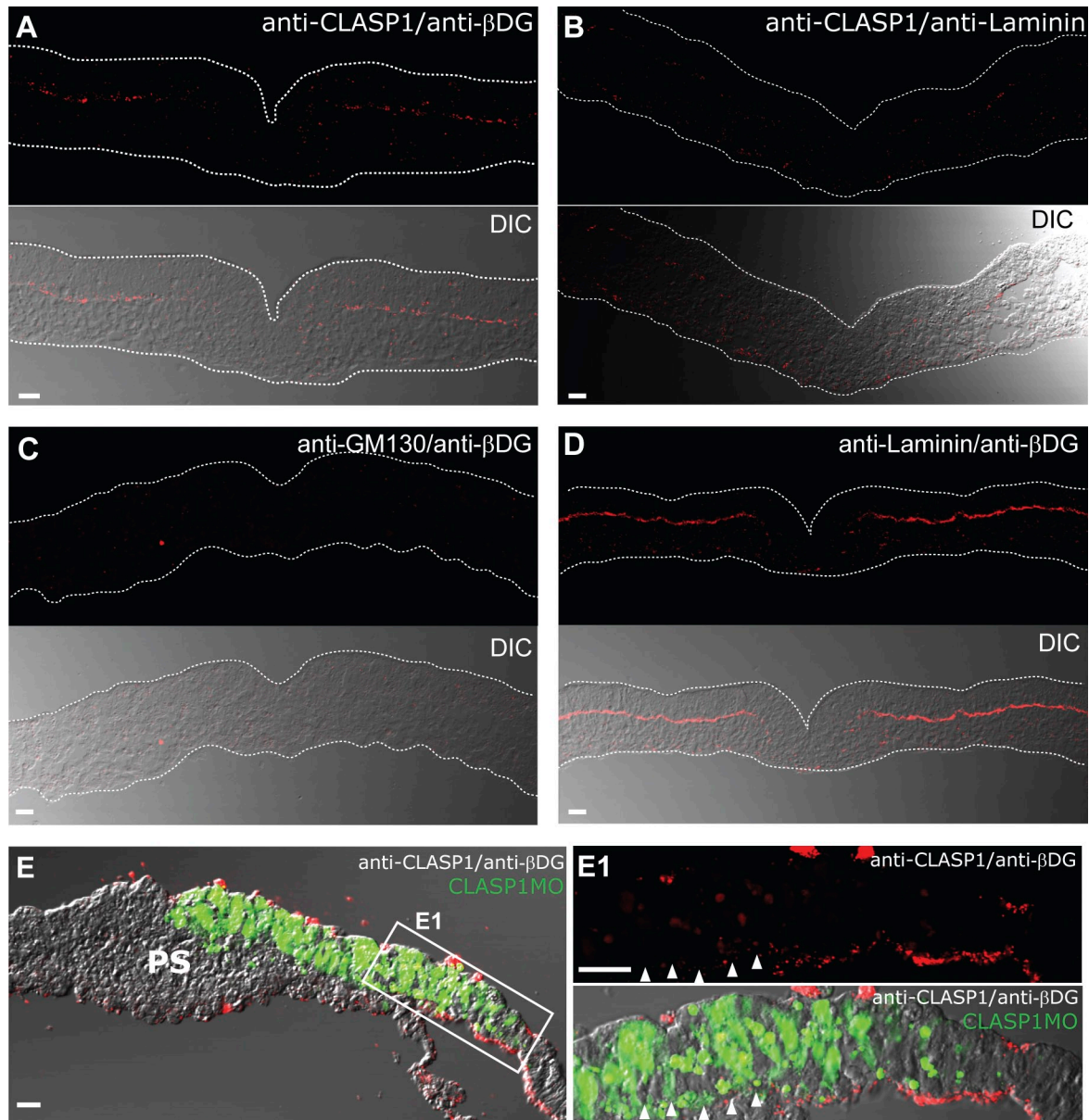
Figure 9. **Proximity ligation analysis reveals an interaction between CLASP and DG in vivo.** (A) Interaction between CLASP1 and βDG in epiblast cells revealed by using the Duolink proximity ligation assay. (B and C) CLASP1/Laminin and GM130/βDG are used as negative controls. (D) Laminin–βDG interaction is used as a positive control. Broken lines indicate the tissue outline (top, apical limit of the epiblast; bottom, apical limit of the endoderm). (E) In epiblast cells electroporated with CLASP1 MO, CLASP1–βDG interaction signals are greatly reduced (arrowheads in E1). Bars, 20 μm.

BM maintenance involves balancing the synthesis and degradation of its components. BM disassembly (breakdown) in streak cells is accompanied by a reduction in component gene expression and an increase in transcripts for many metalloproteinases (Alev et al., 2010; Nakaya et al., 2011; unpublished data). It is unclear whether these transcript-level changes are regulated directly by basal MT dynamics. A more likely scenario is that down-regulation of CLASPs and LL5s, and the resulting MT destabilization, would negatively affect basally targeted secretion of BM proteins and transport of membrane molecules involved in BM–basal membrane interaction. This hypothesis is supported by the fact that secretion and transport of many basolateral membrane and BM proteins are regulated by MT dynamics (Rodriguez-Boulan and Nelson, 1989; De Almeida and Stow, 1991; Teng et al.,

2005; Meng et al., 2008; Wickström et al., 2010), and by our observation that basal DG localization was reduced when CLASP's function or MTs were disrupted (Fig. 8, A and E; Nakaya et al., 2011). Another possible scenario is that the activity of metalloproteinases is negatively regulated by basal MT dynamics. Metalloproteinases are known to play a role in cancer EMTs. In gastrulation EMT, several matrix metalloproteinases and ADAM family metalloproteinases are up-regulated in the primitive streak. Further studies will be needed to show whether their activities (release, activation, etc.) are regulated by changes in basal cortical MTs and basal membrane–BM interaction.

In addition to DG, at least three α integrin (α4, α6, and αV) and three β integrin (β1, β3, and β5) genes are known to be expressed in or around the primitive streak (Nakaya et al., 2011).
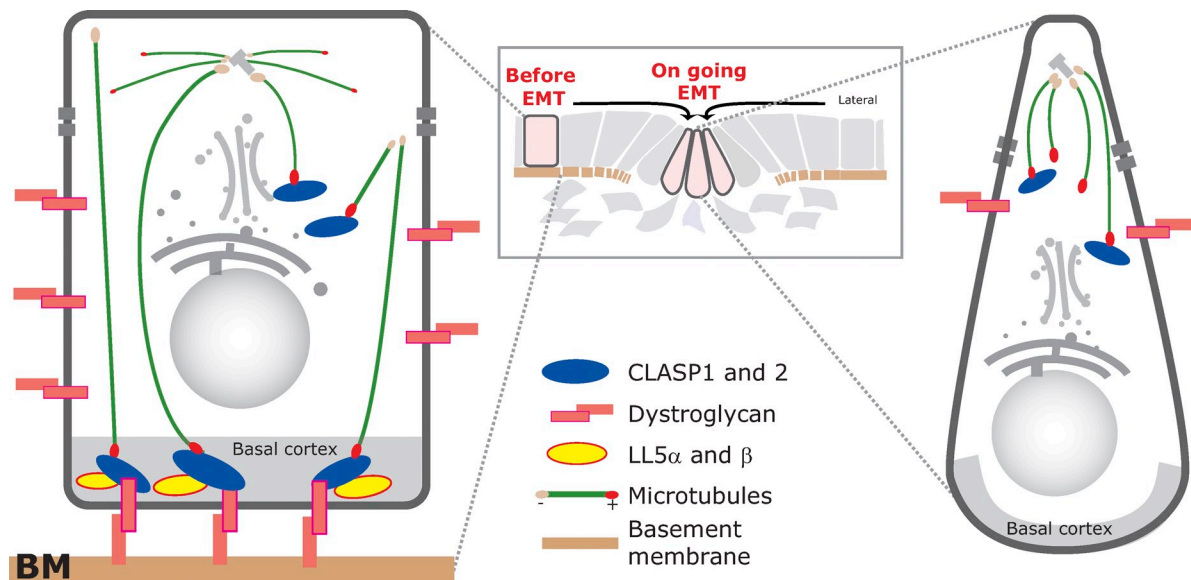
Figure 10.   **A model for the regulation of epiblast cell–BM interaction by CLASP and DG-mediated cortical anchoring of basal MTs during gastrulation EMT.** In epiblast cells before undergoing gastrulation EMT, basal MTs are anchored to and stabilized at the basal cortex through the CLASP–LL5 complex. DG is distributed at the lateral and basal cell membrane, and its basal localization is dependent on basal MT stability and its interaction with the CLASP–LL5 complex. Basal cortical localization of LL5s is largely MT independent, and its interaction with basal membrane proteins like DG and integrins (not depicted) awaits further clarification. It is hypothesized that LL5 basal localization helps enrich and stabilize basal CLASPs and consequently basal MTs. This positive regulatory loop is disrupted as epiblast cells move toward the streak midline, resulting in the loss of basal membrane–BM interaction and consequently BM breakdown.

Integrins, although not being the focus of this work, have also been reported to mediate MT–BM connection through CLASP and LL5 in human mammary epithelial cells (Hotta et al., 2010). A likely scenario during gastrulation EMT is that DG and integrins cooperate in the regulation of basal membrane–BM interaction. Laminin $\alpha 5$, the major α laminin in chicken epiblasts, has been reported to bind $\beta 1$ integrin through its laminin G–like domains 1–3 and to α-DG through its laminin G–like domains 4 and 5 (Yu and Talts, 2003), thus bringing DG and integrins into close physical proximity on the basal membrane. Molecular components associated with each receptor complex likely differ, but their shared intracellular and extracellular interaction partners suggest that functional cross-regulation between these two receptors deserves careful investigation in the future.

By combining eGFP-EB1 electroporation and spinning disk confocal microscopy, we could visualize in this work both apical and basal cortical MT dynamics in live epiblast epithelium. Imaging of live epithelial tissue is often complicated by unique 3D architecture and physiological requirement, and its resolution is generally poor. The chicken epiblast is well-suited for such studies because it is a simple, flat epithelial structure within an embryo of only 4–5 cell-layer thickness. Our time-lapse movies revealed that apical cortical MTs are primarily organized as centrosomal arrays and are dynamic. But most of these MTs appear to terminate at the apical regions of lateral membrane. Basal cortical MTs appear to originate from lateral membrane cortex, which suggests that lateral membrane structures, such as zonula adherens, may serve as noncentrosomal MTOCs for basally targeted MTs. Technical improvement in the future may bring us insight into the architecture and real-time behavior of basal MTs, and on whether they play a role in targeted transport.

Materials and methods

Embryology, microscopy, and immunohistochemistry
Fertilized hens' eggs were purchased from Shiroyama Farm. Embryos were collected from incubated eggs and electroporated using an electroporator (TSS20 Ovodyne; Intracel) with the following parameters: 7 V, 50 ms width, 200 ms internal, three pulses. Embryos were then further grown at 38.5°C using the standard modified New culture method (Nakaya et al., 2008; Alev et al., 2013). Embryos were then analyzed by live imaging or immunofluorescence staining. A laser scanning confocal microscope (FV1000 with BX61WI upright; Olympus) was used for fluorescence microscopy with UPlan-SApochromat 60×/1.2 NA, 40×/0.9 NA, or 20×/0.75 NA objective lenses and Fluoview (Olympus) as the image acquisition software. Olympus SZX12 (for whole-mount) and Olympus BX51 (for sections) microscopes equipped with a DP70 digital camera with a UPlan-SApochromat 20×/0.75 NA lens and DP Controller image acquisition software were used for nonfluorescent imaging. All images were taken at room temperature. For immunohistochemistry, the following primary antibodies were used; Laminin (1:200, laminin-1; 3H11 [Developmental Studies Hybridoma Bank]; L9393 [Sigma-Aldrich]), GFP (1:1,000, A-11122; Invitrogen), Fluorescein/Oregon green–Alexa Fluor 488 conjugate (1:50, A11090; Invitrogen), tetramethylrhodamine (1:50, A6397; Invitrogen), β-DG (1:100; 43DAG1/8D5, NCL-b-DG; Leica), pan–α-tubulin (1:1,000, clone DM1A, T9026; Sigma-Aldrich), and acetylated tubulin (1:1,000, T6793; Sigma-Aldrich). Alexa Fluor 488, 568, 594, or 647 secondary antibodies (1:300 for whole-mount embryo staining, 1:500 for frozen section staining) were used for double or triple color detection. For chemical treatment, embryos were grown in standard New culture setting and treated with Nocodazole (T7402; Sigma-Aldrich) or Cytochalasin D (C8273; Sigma-Aldrich) dissolved in thin albumen at a final concentration of 5 µg/ml. A Duolink proximity ligation assay (#92102; Olink Bioscience; Söderberg et al., 2006) was performed on frozen sections of stage HH4 embryos according to the protocol suggested by the manufacture. A rabbit polyclonal antibody for β-DG (1:100, sc-28535; Santa Cruz Biotechnology, Inc.) was used for this experiment.

Expression constructs and antisense MO oligos
Constructs encoding human CLASP1α, human CLASP2γ and its mutants (ΔMΔC, ΔM, and ΔC), and human LL5α and human LL5β with eGFP tag were provided by Y. Mimori-Kiyosue (Institute of Physical and Chemical Research [RIKEN] Center for Developmental Biology, Kobe, Japan) and A. Akhmanova (Utrecht University, Utrecht, Netherlands; Mimori-Kiyosue

et al., 2005). All fusion proteins were cloned in pEGFP-C1 vector and had an eGFP tag fused at the C terminus. CLASP1α contains amino acid residues 1–1,538 of human CLASP1. CLASP2γ contains amino acid residues 1–1,294 of human CLASP2. CLASP2-ΔM contains amino acid residues 36–340 and 581–1,294 of human CLASP2γ. CLASP2-ΔC contains amino acid residues 36–1,016 of human CLASP2γ. CLASP2-ΔMΔC contains amino acid residues 36–340 and 581–1,016 of human CLASP2γ. Chick full-length DG was cloned into pCAG expression vector, harboring a 2A peptide sequence flanked by multiple cloning sites (a gift from W. Weng (RIKEN Center for Developmental Biology, Kobe, Japan), by PCR with a DNA fragment set of 5′-AATCTAGACGCCACCATGACTGTTG-GATGTGTCCC-3′ and 5′-AATCTAGAAAAGGGGGGACGTAGGGC-GGC-3′. For immunoprecipitation, human DG was obtained from the MGC cDNA library and subcloned into pTARGET vector (Promega), and human CLASP1α and CLASP2γ were subcloned into 3HA-pcDNA expression vector. Fluorescein-tagged CLASP1 translation block MO (1 → 25 of translation initiation junctions), 5′-AGCAGTACTCCATACTGGGCTC-CAT-3′; CLASP2 splicing block MO1 (−12 → 13 of I1E2 junction), 5′-CCAGTAACGCCACCTGTTGAAAAGA-3′; CLASP2 splicing block MO2 (−7 → 18 of E2I2 junction), 5′-AGGTTACTTTTCACTTACCAGTTCC-3′; DG translation block MO (DG-TB; 1 → 25 of translation initiation junctions), 5′-GCTGCGGGACACATCCAACAGTCAT-3′; DG splicing block MO (DG-SB; −9 → 16 of EI2 junction), 5′-CTTCCCAGCTTCGGAGACCTG-GACT-3′; Lissamine-tagged CLASP1 translation block MO (1 → 25 of translation initiation junctions), 5′-AGCAGTACTCCATACTGGGCTCCAT-3′; LL5α translation block MO (−27 → −3 of translation initiation junctions), 5′-GGTCCTTTTCTCCTCCATCCATGTG-3′; LL5β translation block MO (−15 → 10 of translation initiation junctions), 5′-AGAACCCCATCTCTC-CAGCTTTTAT-3′; and standard control MO were purchased from Gene Tools LLC.

In situ hybridization
Probes used for whole-mount in situ hybridization were obtained by RT-PCR using the following primers: chick *CLASP1*, 5′-ATGGAGCCCAGTAT-GGAGTA-3′ (forward) and 5′-TCCCAGTCGTGTTTATCATCA-3′ (reverse), 1,016 bp; chick *CLASP2*, 5′-TGGAATAGCAGACCTACGAGCA-3′ (forward) and 5′-AAGGGTTCCAAAAGTTGCGTGT-3′ (reverse), 1,037 bp; chick *LL5α* (also known as PH-like domain family B, member1 [PHLDB1]; available from GenBank under accession no. XM_417927), 5′-TCGCCT-GATAACATGTCCAGT-3′ (forward) and 5′-TGACGATGACGTCCATC-CAGA-3′ (reverse), 706 bp; and chick *LL5β* (also known as PHLDB2; accession no. XM_416632), 5′-AGCTTCAGCTATCAGATGA-3′ (forward) and 5′-TTACACTGATATAGCCCTCT-3′ (reverse) 1,050 bp. Whole-mount in situ hybridization was performed as described previously (Stern, 1998), and detailed protocol for in situ hybridization can be found elsewhere (Alev et al., 2013). In brief, embryos were fixed in 4% paraformaldehyde at 4°C overnight and stored in 100% methanol at −20°C before in situ hybridization. Embryos in methanol were rehydrated and treated with 10 µg/ml Proteinase K for 15–30 min at room temperature, post-fixed for 30–60 min, prehybridized at 68°C for at least 2 h, and hybridized with gene-specific antisense DIG-labeled probes at 68°C overnight. After hybridization, embryos were washed in prehybridization solution a few times at 68°C and in TBST a few times at room temperature, followed by 2 h of blocking at room temperature, overnight incubation at 4°C in anti-DIG antibody solution, washing, and color development.

Cell culture and immunoprecipitation
The HEK293 cell line was provided by M. Takeichi (RIKEN Center for Developmental Biology). HEK293 cells were cultured in DMEM with 10% FBS and 1% penicillin/streptomycin (Pen Strep; Life Technologies) supplement. Cells were transfected with expression plasmids using FuGENE HD Transfection Reagent (Roche). Immunoprecipitation was performed using Immunoprecipitation kit Dynabeads Protein G (100.07 D; Invitrogen) according to the manufacturer's instructions. In brief, HEK293 cells were lysed in the lysis buffer (50 mM Hepes, pH 7.4, containing 150 mM NaCl, 2 mM EDTA, 1% NP-40, 0.1% SDS, 0.5% sodium deoxycholate, and 1% Triton X-100). Lysates, precleared with protein A/G PLUS Agarose beads (Santa Cruz Biotechnology, Inc.), were incubated for 1 h with anti-HA antibody (16B12, ab24779; Abcam) or anti–β-DG Ab (Leica) that had been coupled to Dynabeads protein G for 1 h. The beads were subsequently washed three times in the wash buffer.

Time-lapse imaging
eGFP-labeled EB1 expression vector only or eGFP-labeled EB1 expression vector plus the mixture of MOs of LL5s and CLASP1 were electroporated into lateral epiblast cells. For time-lapse imaging of EB1 movement, embryos

with mesoderm cells removed by gentle scratching were put on a glass-bottom dish (3960-035; Iwaki), and covered with a cover-glass to avoid drying. Time-lapse imaging was performed using a spinning-disc laser confocal unit CSU-X1 (Yokogawa) with a UPLS-Apochromat 100×/1.40 NA lens and a cooled charge-coupled device camera (ORCA-R2; Hamamatsu Photonics). Images were taken every 1 s for 1 min. Images were reconstituted using MetaMorph software (Molecular Devices).

Online supplemental material
Fig. S1 shows levels of homology between chicken and human CLASPs and the mRNA expression pattern of chicken CLASPs at additional developmental stages. Fig. S2 shows the effects of CLASP2 deletion mutants on laminin expression. Fig. S3 shows mRNA expression of LL5α and LL5β at stage HH4. Fig. S4 shows nocodazole's effect on MT dynamics and MO's effect on CLASP levels and distribution. Fig. S5 shows MO's effect on tubulin and DG distributions. Video 1 shows EB1 dynamics at the apical side of lateral epiblast cells. Video 2 shows EB1 dynamics at the basal side of a control MO cell. Video 3 shows EB1 dynamics at the basal side of a triple MO cell. Videos 4 and 5 show a z-axis sequential view (4) and a 3D view (5) of EB1 signals in a control MO cell. Videos 6 and 7 show a z-axis sequential view (6) and a 3D view (7) of EB1 signals in a triple MO cell. Online supplemental material is available at http://www.jcb.org/cgi/content/full/jcb.201302075/DC1. Additional data are available in the JCB DataViewer at http://dx.doi.org/10.1083/jcb.201302075.dv.

References

Acloque, H., M.S. Adams, K. Fishwick, M. Bronner-Fraser, and M.A. Nieto. 2009. Epithelial-mesenchymal transitions: the importance of changing cell state in development and disease. *J. Clin. Invest.* 119:1438–1449. http://dx.doi.org/10.1172/JCI38019

Akhmanova, A., and C.C. Hoogenraad. 2005. Microtubule plus-end-tracking proteins: mechanisms and functions. *Curr. Opin. Cell Biol.* 17:47–54. http://dx.doi.org/10.1016/j.ceb.2004.11.001

Akhmanova, A., C.C. Hoogenraad, K. Drabek, T. Stepanova, B. Dortland, T. Verkerk, W. Vermeulen, B.M. Burgering, C.I. De Zeeuw, F. Grosveld, and N. Galjart. 2001. Clasps are CLIP-115 and -170 associating proteins involved in the regional regulation of microtubule dynamics in motile fibroblasts. *Cell.* 104:923–935. http://dx.doi.org/10.1016/S0092-8674(01)00288-4

Al-Bassam, J., H. Kim, G. Brouhard, A. van Oijen, S.C. Harrison, and F. Chang. 2010. CLASP promotes microtubule rescue by recruiting tubulin dimers to the microtubule. *Dev. Cell.* 19:245–258. http://dx.doi.org/10.1016/j.devcel.2010.07.016

Alev, C., Y. Wu, T. Kasukawa, L.M. Jakt, H.R. Ueda, and G. Sheng. 2010. Transcriptomic landscape of the primitive streak. *Development.* 137:2863–2874. http://dx.doi.org/10.1242/dev.053462

Alev, C., M. Nakano, Y. Wu, H. Horiuchi, and G. Sheng. 2013. Manipulating the avian epiblast and epiblast-derived stem cells. *Methods Mol. Biol.* In press.

Ayalon, G., J.Q. Davis, P.B. Scotland, and V. Bennett. 2008. An ankyrin-based mechanism for functional organization of dystrophin and dystroglycan. *Cell.* 135:1189–1200. http://dx.doi.org/10.1016/j.cell.2008.10.018

Bacallao, R., C. Antony, C. Dotti, E. Karsenti, E.H. Stelzer, and K. Simons. 1989. The subcellular organization of Madin-Darby canine kidney cells during the formation of a polarized epithelium. *J. Cell Biol.* 109:2817–2832. http://dx.doi.org/10.1083/jcb.109.6.2817

Bozzi, M., S. Morlacchi, M.G. Bigotti, F. Sciandra, and A. Brancaccio. 2009. Functional diversity of dystroglycan. *Matrix Biol.* 28:179–187. http://dx.doi.org/10.1016/j.matbio.2009.03.003

Campbell, K.P. 1995. Three muscular dystrophies: loss of cytoskeleton-extracellular matrix linkage. *Cell.* 80:675–679. http://dx.doi.org/10.1016/0092-8674(95)90344-5

Carvalho, P., J.S. Tirnauer, and D. Pellman. 2003. Surfing on microtubule ends. *Trends Cell Biol.* 13:229–237. http://dx.doi.org/10.1016/S0962-8924(03)00074-6

Cerecedo, D., B. Cisneros, R. Suárez-Sánchez, E. Hernández-González, and I. Galván. 2008. beta-Dystroglycan modulates the interplay between actin and microtubules in human-adhered platelets. *Br. J. Haematol.* 141:517–528. http://dx.doi.org/10.1111/j.1365-2141.2008.07048.x

De Almeida, J.B., and J.L. Stow. 1991. Disruption of microtubules alters polarity of basement membrane proteoglycan secretion in epithelial cells. *Am. J. Physiol.* 261:C691–C700.

Ervasti, J.M., and K.P. Campbell. 1991. Membrane organization of the dystrophin-glycoprotein complex. *Cell.* 66:1121–1131. http://dx.doi.org/10.1016/0092-8674(91)90035-W

Hagedorn, E.J., and D.R. Sherwood. 2011. Cell invasion through basement membrane: the anchor cell breaches the barrier. *Curr. Opin. Cell Biol.* 23:589–596. http://dx.doi.org/10.1016/j.ceb.2011.05.002

Henry, M.D., and K.P. Campbell. 1999. Dystroglycan inside and out. *Curr. Opin. Cell Biol.* 11:602–607. http://dx.doi.org/10.1016/S0955-0674(99)00024-1

Hotta, A., T. Kawakatsu, T. Nakatani, T. Sato, C. Matsui, T. Sukezane, T. Akagi, T. Hamaji, I. Grigoriev, A. Akhmanova, et al. 2010. Laminin-based cell adhesion anchors microtubule plus ends to the epithelial cell basal cortex through LL5α/β. *J. Cell Biol.* 189:901–917. http://dx.doi.org/10.1083/jcb.200910095

Ibraghimov-Beskrovnaya, O., J.M. Ervasti, C.J. Leveille, C.A. Slaughter, S.W. Sernett, and K.P. Campbell. 1992. Primary structure of dystrophin-associated glycoproteins linking dystrophin to the extracellular matrix. *Nature.* 355:696–702. http://dx.doi.org/10.1038/355696a0

Kalluri, R., and R.A. Weinberg. 2009. The basics of epithelial-mesenchymal transition. *J. Clin. Invest.* 119:1420–1428. http://dx.doi.org/10.1172/JCI39104

Kerosuo, L., and M. Bronner-Fraser. 2012. What is bad in cancer is good in the embryo: importance of EMT in neural crest development. *Semin. Cell Dev. Biol.* 23:320–332. http://dx.doi.org/10.1016/j.semcdb.2012.03.010

Lansbergen, G., I. Grigoriev, Y. Mimori-Kiyosue, S. Ohtsuka, S. Higa, I. Kitajima, J. Demmers, N. Galjart, A.B. Houtsmuller, F. Grosveld, and A. Akhmanova. 2006. CLASPs attach microtubule plus ends to the cell cortex through a complex with LL5beta. *Dev. Cell.* 11:21–32. http://dx.doi.org/10.1016/j.devcel.2006.05.012

Levayer, R., and T. Lecuit. 2008. Breaking down EMT. *Nat. Cell Biol.* 10:757–759. http://dx.doi.org/10.1038/ncb0708-757

Lim, J., and J.P. Thiery. 2012. Epithelial-mesenchymal transitions: insights from development. *Development.* 139:3471–3486. http://dx.doi.org/10.1242/dev.071209

Meng, W., Y. Mushika, T. Ichii, and M. Takeichi. 2008. Anchorage of microtubule minus ends to adherens junctions regulates epithelial cell-cell contacts. *Cell.* 135:948–959. http://dx.doi.org/10.1016/j.cell.2008.09.040

Mimori-Kiyosue, Y. 2011. Shaping microtubules into diverse patterns: molecular connections for setting up both ends. *Cytoskeleton (Hoboken).* 68:603–618. http://dx.doi.org/10.1002/cm.20540

Mimori-Kiyosue, Y., I. Grigoriev, G. Lansbergen, H. Sasaki, C. Matsui, F. Severin, N. Galjart, F. Grosveld, I. Vorobjev, S. Tsukita, and A. Akhmanova. 2005. CLASP1 and CLASP2 bind to EB1 and regulate microtubule plus-end dynamics at the cell cortex. *J. Cell Biol.* 168:141–153. http://dx.doi.org/10.1083/jcb.200405094

Moreno-Bueno, G., F. Portillo, and A. Cano. 2008. Transcriptional regulation of cell polarity in EMT and cancer. *Oncogene.* 27:6958–6969. http://dx.doi.org/10.1038/onc.2008.346

Müsch, A. 2004. Microtubule organization and function in epithelial cells. *Traffic.* 5:1–9. http://dx.doi.org/10.1111/j.1600-0854.2003.00149.x

Nakaya, Y., and G. Sheng. 2008. Epithelial to mesenchymal transition during gastrulation: an embryological view. *Dev. Growth Differ.* 50:755–766. http://dx.doi.org/10.1111/j.1440-169X.2008.01070.x

Nakaya, Y., and G. Sheng. 2013. EMT in developmental morphogenesis. *Cancer Lett.* In press. http://dx.doi.org/10.1016/j.canlet.2013.02.037

Nakaya, Y., E.W. Sukowati, Y. Wu, and G. Sheng. 2008. RhoA and microtubule dynamics control cell-basement membrane interaction in EMT during gastrulation. *Nat. Cell Biol.* 10:765–775. http://dx.doi.org/10.1038/ncb1739

Nakaya, Y., E.W. Sukowati, C. Alev, F. Nakazawa, and G. Sheng. 2011. Involvement of dystroglycan in epithelial-mesenchymal transition during chick gastrulation. *Cells Tissues Organs (Print).* 193:64–73. http://dx.doi.org/10.1159/000320165

Patel, K., E. Nogales, and R. Heald. 2012. Multiple domains of human CLASP contribute to microtubule dynamics and organization in vitro and in Xenopus egg extracts. *Cytoskeleton (Hoboken).* 69:155–165. http://dx.doi.org/10.1002/cm.21005

Prins, K.W., J.L. Humston, A. Mehta, V. Tate, E. Ralston, and J.M. Ervasti. 2009. Dystrophin is a microtubule-associated protein. *J. Cell Biol.* 186:363–369. http://dx.doi.org/10.1083/jcb.200905048

Rodriguez-Boulan, E., and W.J. Nelson. 1989. Morphogenesis of the polarized epithelial cell phenotype. *Science.* 245:718–725. http://dx.doi.org/10.1126/science.2672330

Rowe, R.G., and S.J. Weiss. 2009. Navigating ECM barriers at the invasive front: the cancer cell-stroma interface. *Annu. Rev. Cell Dev. Biol.* 25:567–595. http://dx.doi.org/10.1146/annurev.cellbio.24.110707.175315

Schmidt, A., and A. Hall. 2002. The Rho exchange factor Net1 is regulated by nuclear sequestration. *J. Biol. Chem.* 277:14581–14588. http://dx.doi.org/10.1074/jbc.M111108200

Söderberg, O., M. Gullberg, M. Jarvius, K. Ridderstråle, K.J. Leuchowius, J. Jarvius, K. Wester, P. Hydbring, F. Bahram, L.G. Larsson, and U. Landegren. 2006. Direct observation of individual endogenous protein complexes in situ by proximity ligation. *Nat. Methods.* 3:995–1000. http://dx.doi.org/10.1038/nmeth947

Solnica-Krezel, L., and D.S. Sepich. 2012. Gastrulation: making and shaping germ layers. *Annu. Rev. Cell Dev. Biol.* 28:687–717. http://dx.doi.org/10.1146/annurev-cellbio-092910-154043

Stern, C.D. 1998. Detection of multiple gene products simultaneously by in situ hybridization and immunohistochemistry in whole mounts of avian embryos. *Curr. Top. Dev. Biol.* 36:223–243. http://dx.doi.org/10.1016/S0070-2153(08)60505-0

Teng, J., T. Rai, Y. Tanaka, Y. Takei, T. Nakata, M. Hirasawa, A.B. Kulkarni, and N. Hirokawa. 2005. The KIF3 motor transports N-cadherin and organizes the developing neuroepithelium. *Nat. Cell Biol.* 7:474–482. http://dx.doi.org/10.1038/ncb1249

Thiery, J.P., H. Acloque, R.Y. Huang, and M.A. Nieto. 2009. Epithelial-mesenchymal transitions in development and disease. *Cell.* 139:871–890. http://dx.doi.org/10.1016/j.cell.2009.11.007

Wen, Y., C.H. Eng, J. Schmoranzer, N. Cabrera-Poch, E.J. Morris, M. Chen, B.J. Wallar, A.S. Alberts, and G.G. Gundersen. 2004. EB1 and APC bind to mDia to stabilize microtubules downstream of Rho and promote cell migration. *Nat. Cell Biol.* 6:820–830. http://dx.doi.org/10.1038/ncb1160

Wickström, S.A., A. Lange, M.W. Hess, J. Polleux, J.P. Spatz, M. Krüger, K. Pfaller, A. Lambacher, W. Bloch, M. Mann, et al. 2010. Integrin-linked kinase controls microtubule dynamics required for plasma membrane targeting of caveolae. *Dev. Cell.* 19:574–588. http://dx.doi.org/10.1016/j.devcel.2010.09.007

Williams, M., C. Burdsal, A. Periasamy, M. Lewandoski, and A. Sutherland. 2012. Mouse primitive streak forms in situ by initiation of epithelial to mesenchymal transition without migration of a cell population. *Dev. Dyn.* 241:270–283. http://dx.doi.org/10.1002/dvdy.23711

Yu, H., and J.F. Talts. 2003. Beta1 integrin and alpha-dystroglycan binding sites are localized to different laminin-G-domain-like (LG) modules within the laminin alpha5 chain G domain. *Biochem. J.* 371:289–299. http://dx.doi.org/10.1042/BJ20021500